Capabilities of time-resolved X-ray excited optical luminescence of the Taiwan Photon Source 23A X-ray nanoprobe beamline

Bi-Hsuan Lin,[a]* Yu-Hao Wu,[a] Xiao-Yun Li,[a] Hsu-Cheng Hsu,[b] Yu-Cheng Chiu,[c] Chien-Yu Lee,[a] Bo-Yi Chen,[a] Gung-Chian Yin,[a] Shao-Chin Tseng,[a] Shih-Hung Chang,[a] Mau-Tsu Tang[a] and Wen-Feng Hsieh[d]

[a]National Synchrotron Radiation Research Center, Hsinchu 30076, Taiwan, [b]Department of Photonics, National Cheng Kung University, Tainan 70101, Taiwan, [c]Department of Chemical Engineering, National Taiwan University of Science and Technology, Taipei 10607, Taiwan, and [d]Department of Photonics and Institute of Electro-Optical Engineering, National Chiao Tung University, Hsinchu 30010, Taiwan. *Correspondence e-mail: bihsuan@nsrrc.org.tw

Time-resolved X-ray excited optical luminescence (TR-XEOL) was developed successfully for the 23A X-ray nanoprobe beamline located at the Taiwan Photon Source (TPS). The advantages of the TR-XEOL facility include (i) a nano-focused X-ray beam (<60 nm) with excellent spatial resolution and (ii) a streak camera that can simultaneously record the XEOL spectrum and decay time. Three time spans, including normal (30 ps to 2 ns), hybrid (30 ps to 310 ns) and single (30 ps to 1.72 µs) bunch modes, are available at the TPS, which can fulfil different experimental conditions involving samples with various lifetimes. It is anticipated that TR-XEOL at the TPS X-ray nanoprobe could provide great characterization capabilities for investigating the dynamics of photonic materials.

1. Introduction

X-ray excited optical luminescence (XEOL) (Nie *et al.*, 2017; Ma *et al.*, 2019; Novais *et al.*, 2012; Salomon *et al.*, 2017) is a well developed and advanced characterization technique employed at synchrotron radiation facilities. Although this method involves a relatively simple X-ray-photon-in/optical-photon-out measurement, XEOL is a promising technique for investigating optical decay channels and their relationship with specific absorption processes at the core level (Sham *et al.*, 1993; Ward *et al.*, 2013; Heigl *et al.*, 2007). In synchrotron source pumping, the X-ray energy can be tuned across the absorption edge of a specific element of the sample to study its emission properties. According to the report of Sham & Rosenberg (2007) the tunable synchrotron source can create an excited state to decay optically via more pathways through exciting the core-to-continuum, core-to-quasi-bound and core-to-bound transitions. Using the high-energy resolution of the synchrotron source, different chemical sites or polytypes of the same element can also be sensitive to a specific channel via selective excitation. Time-resolved XEOL (TR-XEOL) could be developed to investigate the luminescence dynamic process of materials, as the synchrotron source offers the advantage of good temporal domain measurements. TR-XEOL can be performed at several synchrotron facilities, including the Canadian Light Source (CLS) (Sham, 2014; Armelao *et al.*, 2010), European Synchrotron Radiation Facility (ESRF) (Martínez-Criado *et al.*, 2014), Advanced Photon Source (APS) (Heigl *et al.*, 2007; Sham & Rosenberg, 2007), Cornell High Energy Synchrotron Source (CHESS)
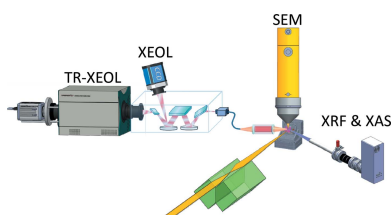
(O'Malley *et al.*, 2011) and Diamond Light Source (DLS) (Taylor *et al.*, 2013; Mosselmans *et al.*, 2013). Based on the requirements of previous research studies, a TR-XEOL facility was created for the 23A X-ray nanoprobe beamline located at the Taiwan Photon Source (TPS) at the National Synchrotron Radiation Research Center of Taiwan. The pulse duration of the TPS is ∼30 ps, which was measured by Liao *et al.* (2015). Three different filling patterns of the electron bunches can be applied at the TPS: single, normal and hybrid bunch modes, which provide time scales of 30 ps to 1.72 μs, 30 ps to 2 ns and 30 ps to 310 ns, respectively. Thus, a suitable time scale can be selected based on the desired TR-XEOL experiments. In this report, the capabilities of TR-XEOL at the TPS 23A beamline were evaluated using three test samples, *i.e.* trihalide perovskite $CH_3NH_3PbBr_3$ (Kumar *et al.*, 2016), a single ZnO microrod (Lin *et al.*, 2019) and a *c*-plane ZnO wafer (Lin *et al.*, 2016), to demonstrate TR-XEOL operation in the single, normal and hybrid bunch modes, respectively. Furthermore, the advantages of using the streak camera as a detector will also be discussed.

2. Experimental setup and results

2.1. Endstation functions

The TPS 23A X-ray nanoprobe is a multifunctional hard X-ray (4–15 keV) beamline. Fig. 1 shows a schematic of the experimental setup and associated functions. The X-ray beam was focused using Montel mirrors (Ice *et al.*, 2011; Yin *et al.*, 2016), which can deliver X-ray beam spot sizes of less than 60 nm. However, according to results from Rogalev & Goulon (2002), the spatial resolution at these X-ray energies will be limited by secondary excitations created by the X-rays to 150–200 nm. The sample was mounted on a piezo flexure stage with fine and coarse alignments, which provide traveling ranges of 100 μm and 25 mm, respectively. A three-axis laser interferometer was used to precisely monitor the position of the sample stage in the 2D mapping measurements with on-the-fly scanning (Lee *et al.*, 2018). X-ray absorption spectroscopy
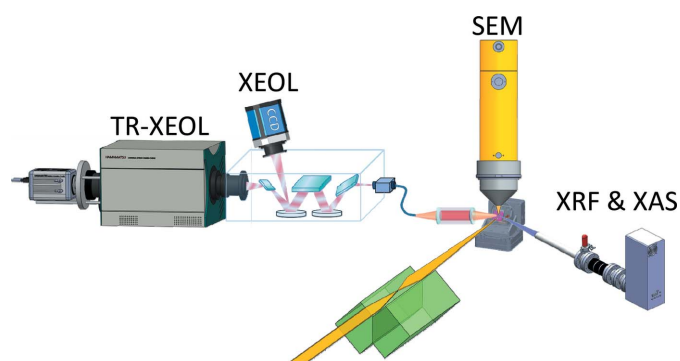

Figure 1
The main functions of the X-ray nanoprobe at the TPS 23A beamline located at the Taiwan Photon Source, including XEOL, TR-XEOL, XRF, XAS and CL. The measured sample will be equipped in the environment of a high vacuum (1×10^{-6} torr) and room temperature (300 K) with a load-lock system to quickly transfer the samples between the main chamber and the preparation chamber.

(XAS) and X-ray fluorescence (XRF) were conducted using a silicon drift detector (SDD; Vortex-ME4, HITACHI). The TR-XEOL was collected by a 10 m fiber and directed to a spectrometer (iHR320, HORIBA) equipped with a Hamamatsu C10910 streak camera and M10913 slow single sweep unit. A Stanford Research Systems DG645 delay generator was used, operating with a jitter of ∼25 ps. Typical image magnifications for input optics, streak tube and output optics of the streak camera are 1:1, 1:2.8 and 1:0.7, respectively. The CCD of the streak camera has 1344 (horizontal for wavelength) × 1024 (vertical for time) pixels with a cell size of 6.45 μm × 6.45 μm. In this case, for a streak image with 2 ns sweep time and with the streak slit opened to 40 μm, we calculated the related resolution to be about 24 ps for the detector. Concerning the resolution of the TR-XEOL, one should consider the instrument response function (IRF). The IRF has three main factors: the pulsed duration times of the source (τ_s), the electronics (τ_e) and the detector (τ_d), and can be approximated as IRF $\cong [(\tau_s)^2 + (\tau_e)^2 + (\tau_d)^2]^{1/2}$. We can then calculate the IRF to be 45 ps, using $\tau_s \cong 30$ ps, $\tau_e \cong 25$ ps and $\tau_d \cong 24$ ps in the case of a streak image with 2 ns sweep time.

The XEOL was also collected by an optical fiber and directed to another spectrometer (iHR550, HORIBA) with a liquid-nitrogen-cooled charge-coupled device (CCD; BIUV Symphony II) with a resolution of 2048 × 512 pixels. The iHR550 spectrometer was equipped with a photomultiplier tube (PMT) and switching mirror, which could be used to perform XEOL mapping. The collected emission wavelengths of both TR-XEOL and XEOL ranged from 200 nm to 1000 nm. A scanning electron microscope (SEM) was also installed at the endstation to quickly identify sample positions. Additionally, the SEM could also be used for scanning cathodoluminescence (CL) as a complementary method to analyze the emission properties of materials (Lin *et al.*, 2019).

2.2. Single bunch mode

Fig. 2 shows the capabilities of XRF and XEOL mapping with 13.5 keV X-rays (above the Br *K*-edge and Pb *L₃*-edge at 13.474 keV and 11.035 keV, respectively). The elemental distributions of the trihalide perovskite $CH_3NH_3PbBr_3$ corresponding to Pb and Br are shown in Figs. 2(*a*) and 2(*b*), respectively, while the XEOL spectrum and maps of the related emissions are shown in Figs. 2(*c*) and 2(*d*). The XEOL spectrum indicates that the main emission peak had a wavelength of ∼535 nm. The results clearly show the elemental distributions and their corresponding emission peaks. The XRF and XEOL maps could be measured simultaneously in one scan. All emission lines under 13.5 keV were recorded by a silicon drift detector and plotted using the beamline software (Lee *et al.*, 2018).

Luminescence dynamics of the trihalide perovskite $CH_3NH_3PbBr_3$ were measured using TR-XEOL in the single bunch mode, as shown in Fig. 3. The TPS has a circumference of ∼518 m, with an available time scale of ∼1.72 μs (578 kHz) in the single bunch mode and beam current of 2 mA. Thus, the
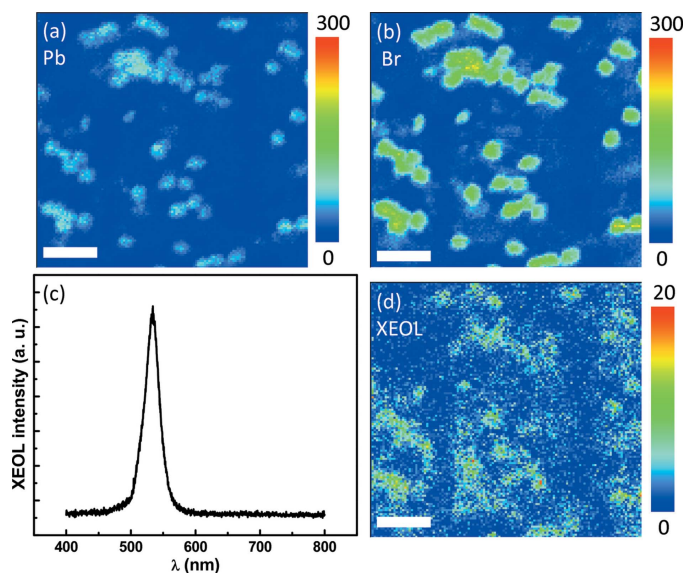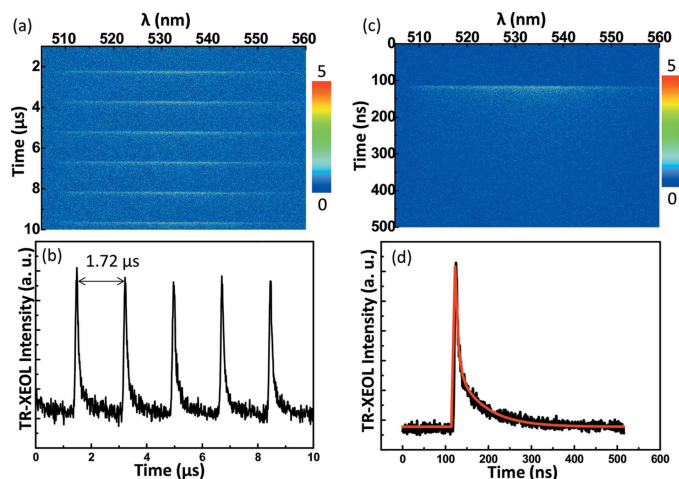
Figure 2
X-ray fluorescence maps of elements (*a*) Pb and (*b*) Br. The X-ray excited optical luminescence (XEOL) spectrum and perovskite map are shown in (*c*) and (*d*), respectively. All scale bars correspond to 10 μm.

Figure 3
The streak image and corresponding spectral integrated time trace are shown in panels (*a*) and (*b*), respectively, obtained using a streak camera with a 10 μs time span, highlighting the 1.72 μs period of the single bunch mode. A 500 ns time span was used to obtain further information on the luminescence dynamics of the perovskite, creating the (*c*) streak image and (*d*) lifetime obtained by fitting the TR-XEOL trace.

repetition rate of the M10913 slow single sweep unit was set to 578 kHz in the external rising mode in the TR-XEOL experiments. Fig. 3(*a*) shows the streak image recorded with a 10 μs sweep time, while its spectral integrated (510–530 nm) time trace is shown in Fig. 3(*b*). Five repeated risings can be observed where the interval time of each rising was 1.72 μs. This clearly demonstrates that the electron filling pattern was operated in the single bunch mode. The sweep time of the streak image can be tuned to a suitable range, for example to 500 ns as shown in Fig. 3(*c*) for the TR-XEOL measurements. The spectral integrated (510–530 nm) time traces were fitted using two exponential decay functions, as shown in Fig. 3(*d*), to obtain decay lifetimes of $\tau_1 \simeq$ 6 ns and $\tau_2 \simeq$ 64 ns.

2.3. Normal bunch mode

As the electron RF-cavity of the TPS was operated at 500 MHz (2 ns), the normal bunch mode could apply a time scale of 30 ps to 2 ns. Therefore, materials with a faster decay lifetime (<2 ns) could be measured using TR-XEOL at the TPS 23A beamline. The repetition frequency of TR-XEOL was set to 3.469 MHz (499.665 MHz/144) in the normal bunch mode, as the maximal sweep repetition frequency of the M10913 slow single sweep unit was 4 MHz. In our previous report (Lin *et al.*, 2019), we observed that the near band edge (NBE) emission intensity of a single ZnO microrod increased

nonlinearly with the XAS fluorescence yield. Thus, the luminescence dynamics of a single ZnO microrod can be investigated further using TR-XEOL. The single ZnO microrod and its Zn *K*-edge XAS spectra are shown in Figs. 4(*a*) and 4(*b*), respectively. This indicates the convenience of using SEM at the TPS 23A beamline to identify the sample quickly, and the advantages of using tunable and continuous X-ray energy set across the Zn *K*-edge to study the luminescence dynamics. Figs. 4(*c*) and 4(*d*) show the streak images recorded with a 2 ns sweep time and the corresponding spectral integrated (360–
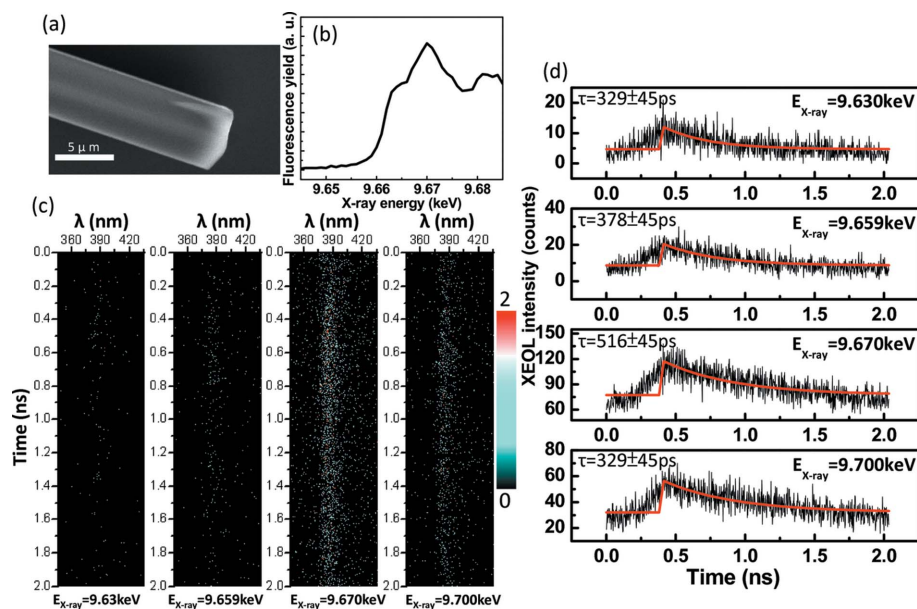
Figure 4
(*a*) SEM image and (*b*) Zn *K*-edge XAS for the single ZnO microrod. (*c*) The corresponding TR-XEOL streak images with X-ray energies set across the Zn *K*-edge and (*d*) the lifetimes obtained by fitting the TR-XEOL traces of (*c*).

420 nm) time traces of the single ZnO microrod. After fitting the spectral integrated time traces using a single exponential function, we obtained decay lifetimes of 329 ± 45 ps, 378 ± 45 ps, 516 ± 45 ps and 329 ± 45 ps for the 9.630 keV, 9.659 keV, 9.670 keV and 9.700 keV X-ray energy excitations, respectively. It can be observed that the decay lifetime shows a similar positive edge jump following XAS across the Zn K-edge. This indicates that the XEOL of the single ZnO microrod had the longest decay lifetime when pumped at the resonant energy (9.670 keV) and shorter decay lifetimes when excited to levels either below or above the Zn K-edge. We believe that this behavior was due to the high volumetric carrier densities caused by the pulsed X-rays at the resonant energy, which excited more free carriers compared with those excited below and above the Zn K-edge energies. The peak power density of TPS 23A beamline is about ∼30 MW cm^{-2} (repetition rate 500 MHz, X-ray peak duration time 30 ps, photon flux 10^{10} photons s^{-1} and X-ray spot size ∼60 nm at 10 keV), which is about seven orders of magnitude larger than that of an unfocused X-ray beam (∼6 W cm^{-2}). This finding was consistent with our previous reports where the pulsed X-rays excited the high-density low-energy free carriers at the resonant energy of the Zn K-edge, resulting in Coulomb screening of the spontaneous polarization. This decreased the exciton–phonon interactions, causing a spectral blue shift of 40–50 meV in the ZnO wafers (Lin *et al.*, 2016, 2018). As the cooling of the hot carriers depended on interactions with the phonons, the reduced exciton–phonon interactions caused a slower decay of the free carriers.

On the other hand, the decay curve measurements of Fig. 4(*d*) show similar odd pre-excitation shoulders, which may be caused by chromatic dispersion from the optical fiber. TR-XEOL is still in the early stage of development at the TPS 23A beamline; a more quantitative comparison with conventional methods requires further studies. A better data quality may be obtained by shortening the length of the optical fiber, and a good fitting technique will be learned from the fluorescence lifetime imaging community.

2.4. Hybrid bunch mode

The hybrid bunch mode was developed successfully at the TPS. The advantages of operating in the hybrid bunch mode are: (i) the electron beam current can reach 400 mA, providing high X-ray photon flux, and (ii) the longer time interval can facilitate temporal domain measurements. There are ∼864 electron bunches in the storage ring of the TPS, which have a minimum interval of 2 ns. In our hybrid bunch mode, we could achieve ∼155 symmetric electron bunches to obtain a ∼310 ns interval between the single and multi-electron bunches. Figs. 5(*a*) and 5(*b*) show the streak images recorded with a 2 µs sweep time and the corresponding spectral integrated (380–400 nm) time trace, respectively, of the *c*-plane ZnO wafer operating in the hybrid bunch mode. The time interval of the hybrid bunch mode was appropriate, as the decay lifetime of the *c*-plane ZnO was approximately hundreds of picoseconds. The streak image shown in Fig. 4(*a*) was measured at 578 kHz
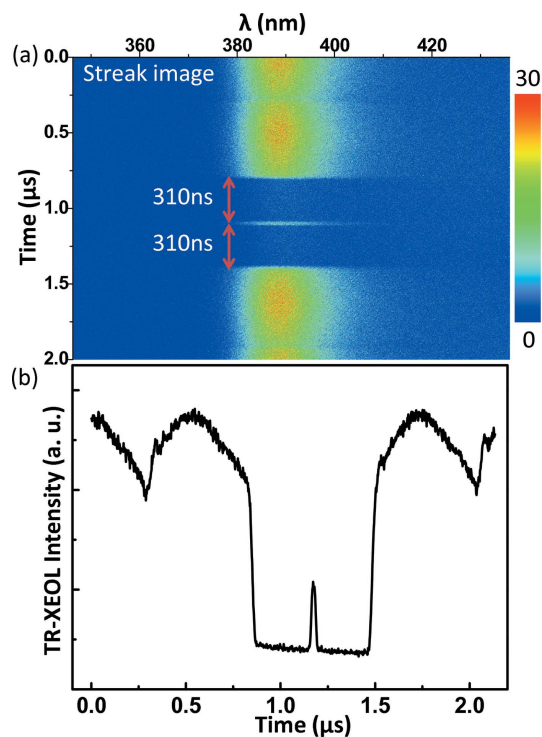

Figure 5
The streak image (*a*) and spectral integrated time trace (*b*) in the hybrid bunch mode.

(499.665 MHz/864), which could provide a time interval of 30 ps to 310 ns. The hybrid bunch mode still had electron bunches with 2 ns intervals, so a repetition rate of 3.469 MHz (499.665 MHz/144) could also be used for time intervals of 30 ps to 2 ns, depending on user demand.

3. Conclusions

TR-XEOL capabilities were developed successfully for the TPS 23A beamline. The advantages of TR-XEOL include the following: (i) the nano-focused X-ray beam (<60 nm) offers excellent spatial resolution, and (ii) a streak camera can be employed to simultaneously record the XEOL emission spectrum and decay time. Three time intervals, including normal (30 ps to 2 ns), hybrid (30 ps to 310 ns) and single (30 ps to 1.72 µs) bunch modes, are available to provide different experimental conditions to test samples with various emission lifetimes. The hybrid bunch, in particular, provides a high X-ray photon flux, which fulfils the requirements for a multi-functional beamline and the wide time spans necessary for taking temporal domain measurements. We anticipate that TR-XEOL at the TPS X-ray nanoprobe will offer powerful characterization capabilities for investigating the dynamics of photonic materials.

Funding information

References

Armelao, L., Heigl, F., Brunet, S., Sammynaiken, R., Regier, T., Blyth, R. I., Zuin, L., Sankari, R., Vogt, J. & Sham, T. K. (2010). *ChemPhysChem*, **11**, 3625–3631.

Heigl, F., Jürgensen, A., Zhou, X.-T., Lam, S., Murphy, M., Ko, J. Y. P., Sham, T. K., Rosenberg, R. A., Gordon, R., Brewe, D., Regier, T. & Armelao, L. (2007). *AIP Conf. Proc.* **879**, 1202–1205.

Ice, G. E., Budai, J. D. & Pang, J. W. L. (2011). *Science*, **334**, 1234–1239.

Kumar, S., Jagielski, J., Yakunin, S., Rice, P., Chiu, Y.-C., Wang, M., Nedelcu, G., Kim, Y., Lin, S., Santos, E. J., Kovalenko, M. V. & Shih, C. J. (2016). *ACS Nano*, **10**, 9720–9729.

Lee, C.-Y., Yin, G.-C., Chen, B.-Y., Chen, H.-Y., Lin, B.-H., Tseng, S.-C., Chang, S.-H., Li, X.-Y. & Tang, M.-T. (2018). *Microsc. Microanal.* **24**, 106–107.

Liao, C.-Y., Wu, C.-Y., Cheng, Y.-S., Kuan, C.-K., Chuang, J.-Y., Hsueh, H.-P., Hsu, S.-Y., Hu, K. H. & Hsu, K. T. (2015). *Proceedings of the Sixth International Particle Accelerator Conference (IPAC2015)*, 3–8 May 2015, Richmond, VA, USA, pp. 1109–1111. MOPTY074.

Lin, B. H., Chen, H.-Y., Tseng, S.-C., Wu, J.-X., Chen, B.-Y., Lee, C.-Y., Yin, G.-C., Chang, S.-H., Tang, M.-T. & Hsieh, W. F. (2016). *Appl. Phys. Lett.* **109**, 192104.

Lin, B.-H., Li, X.-Y., Lin, D.-J., Jian, B.-L., Hsu, H.-C., Chen, H.-Y., Tseng, S.-C., Lee, C.-Y., Chen, B.-Y., Yin, G.-C., Hsu, M. Y., Chang, S. H., Tang, M. T. & Hsieh, W. F. (2019). *Sci. Rep.* **9**, 207.

Lin, B.-H., Wu, Y.-C., Chen, H.-Y., Tseng, S.-C., Wu, J.-X., Li, X.-Y., Chen, B.-Y., Lee, C.-Y., Yin, G.-C., Chang, S.-H., Tang, M.-T. & Hsieh, W. F. (2018). *Opt. Express*, **26**, 2731–2739.

Ma, J., Yao, Q., McLeod, J. A., Chang, L.-Y., Pao, C.-W., Chen, J., Sham, T.-K. & Liu, L. (2019). *Nanoscale*, **11**, 6182–6191.

Martínez-Criado, G., Segura-Ruiz, J., Alén, B., Eymery, J., Rogalev, A., Tucoulou, R. & Homs, A. (2014). *Adv. Mater.* **26**, 7873–7879.

Mosselmans, J., Taylor, R., Quinn, P., Finch, A., Cibin, G., Gianolio, D. & Sapelkin, A. (2013). *J. Phys. Conf. Ser.* **425**, 182009.

Nie, Y., Wang, Z., Wang, J., Bao, F., Zhang, J., Ma, Y., Sham, T.-K. & Sun, X. (2017). *J. Phys. Chem. C*, **121**, 26076–26085.

Novais, S. M. V., Valerio, M. E. G. & Macedo, Z. S. (2012). *J. Synchrotron Rad.* **19**, 591–595.

O'Malley, S. M., Revesz, P., Kazimirov, A. & Sirenko, A. A. (2011). *J. Appl. Phys.* **109**, 124906.

Rogalev, A. & Goulon, J. (2002). *Chemical Applications of Synchrotron Radiation, Part II: X-ray Applications*, pp. 707–760. Singapore: World Scientific.

Salomon, D., Messanvi, A., Eymery, J. & Martínez-Criado, G. (2017). *Nano Lett.* **17**, 946–952.

Sham, T. K. (2014). *Adv. Mater.* **26**, 7896–7901.

Sham, T. K., Jiang, D. T., Coulthard, I., Lorimer, J. W., Feng, X. H., Tan, K. H., Frigo, S. P., Rosenberg, R. A., Houghton, D. C. & Bryskiewicz, B. (1993). *Nature*, **363**, 331–334.

Sham, T. K. & Rosenberg, R. A. (2007). *ChemPhysChem*, **8**, 2557–2567.

Taylor, R. P., Finch, A. A., Mosselmans, J. F. W. & Quinn, P. D. (2013). *J. Lumin.* **134**, 49–58.

Ward, M. J., Regier, T. Z., Vogt, J. M., Gordon, R. A., Han, W. Q. & Sham, T. K. (2013). *J. Phys. Conf. Ser.* **425**, 092006.

Yin, G.-C., Chang, S.-H., Chen, B.-Y., Chen, H.-Y., Lin, B.-H., Tseng, S.-C., Lee, C.-Y., Wu, J.-X., Wu, S.-Y. & Tang, M.-T. (2016). *AIP Conf. Proc.* **1741**, 030004.